# Experimental performance of a field of parabolic trough collectors for small-scale power generation

***Rémi Dickes[a,*], Olivier Dumont[a], Jérémie Thiébaut[a], Matthew Orosz[b,d], Amy Mueller[c,d] and Vincent Lemort[a]***

*[a] Thermodynamics Laboratory, University of Liège, Liège, Belgium*
*[b] Massachusetts Institute of Technology, Cambridge, USA*
*[c] Northeastern University, Boston, USA*
*[d] STG International, Cambridge, USA / Maseru , Lesotho*

*[*] Corresponding author: rdickes@ulg.ac.be*

**Abstract:**

The present work investigates the solar field performance of a pilot system installed at the University of Liège in Belgium. The system includes eight parabolic trough collectors connected in series (66m² in total) and is aimed for small-scale power generation (2kWe) at low-temperature operation (150°C max.). The paper describes the test facility and presents experimental data gathered under various operating conditions. After posttreatment, the measurements are used to calibrate a deterministic model of the solar collectors. This model is used to better estimate the various sources of losses during the solar energy conversion and to investigate potential means of performance improvements. While the collection efficiency recorded experimentally does not exceed 30%, it is shown that an improvement of the tracking could raise this value to 65% and thus meet the design expectations.

**Keywords:**

PTC, parabolic trough, solar collectors, experimental

# 1. Introduction

Solar-powered organic Rankine cycles (ORC) exist since the late 19th century [1]. Aiming to convert low-temperature solar resource into useful work, solar ORCs have been developed for multiple applications, including irrigation [2], desalination [3], domestic CHP [4] or power generation purposes [5]. Since 2010, the University of Liège is developing such a micro-scale solar thermal power plant for both pedagogical and research purposes. Named *Sun2Power*, the system includes a field of parabolic trough collectors (PTCs), a single-tank storage and an organic Rankine cycle unit for converting low-grade heat into electricity. Developed, sized, built and operated by engineering students of the University of Liège, this solar system aims to offer a practical case study for training the students during their formation. While extensive investigations on the ORC unit have been presented in previous works [6]–[8], this paper presents the first experimental feedback gathered on the Sun2Power solar field. More specifically, this contribution aims to analysis the recorded performance, to identify the main sources of losses, and to investigate the potential means for improving the solar field efficiency.

To this end, the paper is structured as follows: firstly, the test rig and its main subcomponents (i.e. the solar collectors, the HTF circuit and the acquisition system) are described in Section 2. In Section 3, experimental measurements gathered with the solar field are presented and discussed. Using these data, a deterministic model of the PTC is presented and calibrated in Section 4. Ultimately, the model is used to extrapolate the solar field performance and investigate potential means of improvements.

## 2. System description

The following section describes the *Sun2Power* solar field and its subsystems as installed at the University of Liège (50.586°N/5.565°E). The solar field is depicted in Fig. 1 and a summary of the most representative properties of the system is given in Appendix.

*Fig. 1. Photos of the Sun2Power solar field in operation (August 2017 – Liège, Belgium).*

### 2.1 Solar collectors

The *Sun2Power* solar field consists of two rows of four parabolic trough collectors connected in series, resulting in a total effective aperture of 65.6m². The eight collectors are T13 modules developed by STG International, a non-profit organization undertaking development and deployment of renewable energy technologies appropriate for use in rural areas of developing countries [9], [10]. As depicted in Fig. 2a, each collector consists of two symmetrical reflector panels that snap into two structural support rings. The reflective surface of the panels is Miro4 [11] while a black-painted steel tube is used as receiver pipe along the collectors focal line. In order to reduce heat losses to the ambiance, a borosilicate glazing envelope (with an air-filled annulus) is placed around the absorber tubes. As shown in Fig. 3, the glass envelope is maintained concentric to the absorber tube by means of PTFE bushings. To account for any dilatation difference between the steel pipe and the glass envelope during operation, the PTFE bushings are maintained in position by pre-stressed springs preventing the envelope falling on the steel pipe.

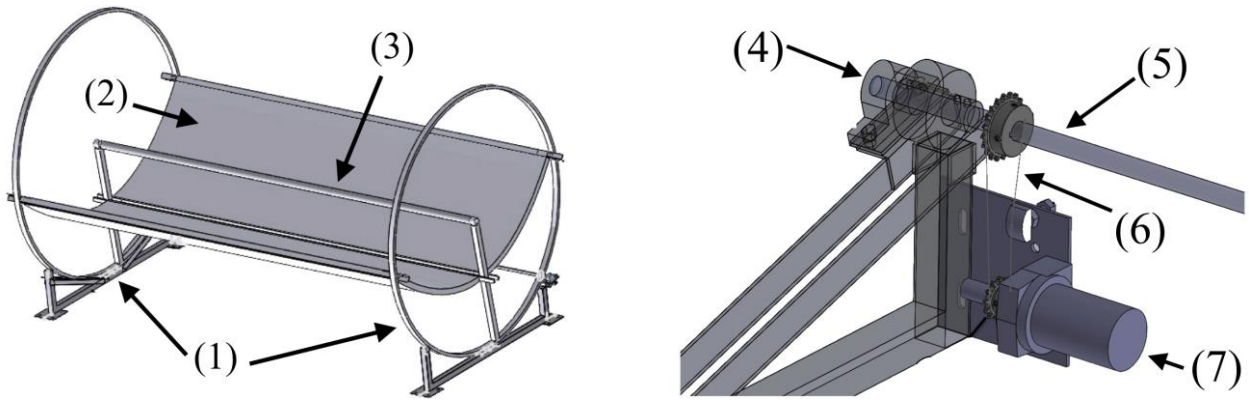


*Fig. 2. a) CAD scheme of one T13 module. b) zoom-in view of the tracking mechanism.* [10]
*(1) support rings (2) reflector panels (3) receiver pipe (4) drive roller (5) drive shaft (6) roller chain (7) drive motor.*

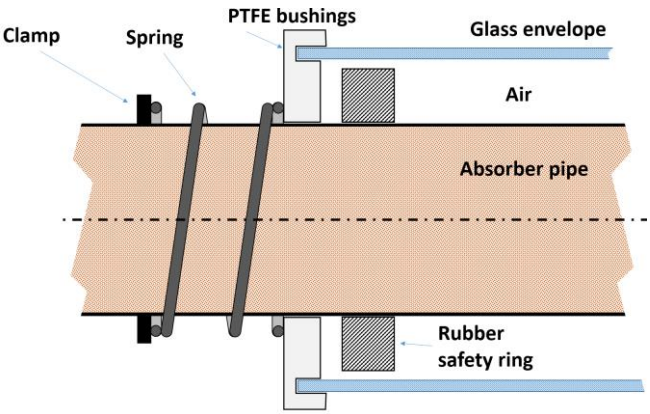


*Fig. 3. Zoom-in view of the heat collection elements and the PTFE bushings* [12]

Oriented in a North-South alignment, the solar field features a single-axis tracking mechanism to follow the East-to-West motion of the Sun during the day. For each row individually, the PTCs rotation is actuated by peripheral drive rollers onto which are placed the structural support rings. These rollers are connected to a mechanical shaft, which is itself turned by a single 12 DC motor via a roller chain (see Fig. 2b). Rotation can either be automated or manually-controlled through an Arduino user interface. In case of automated control, the Arduino program implements the NREL Sun Position Algorithm [13] and drives the PTCs using the feedback from an inclinometer sensors placed on each row. More specifically, the controller adjust the position of each row individually until the solar field is "in focus", i.e.

$$|\theta_{Sun} - \theta_{PTC}| \leq \alpha_{tracking} \ , \qquad (1)$$

where $\theta_{Sun}$ is the target angle pointing toward the Sun, $\theta_{PTC}$ is the actual position of the collectors as measured by the inclinometers, and $\alpha_{tracking}$ is a tolerance angle to adjust in the controller.

## 2.2 HTF circuit

The solar collectors are part of a global heat transfer circuit as illustrated in Fig. 4. The heat transfer fluid (HTF) is thermal oil *HTF-Basic* from Pirobloc [14] and it is pumped through the system by means of a speed-controlled NG11V-PH gear pump [15]. A single tank is placed at the solar field outlet to play the dual role of buffer tank and HTF storage reservoir when the system is not in operation. Although aimed to be connected with a 2kWe ORC unit, preliminary tests of the solar field are performed using an air-cooled heat exchanger (HEX) as thermal load. The air flow drawn through the HEX is controlled by means of a variable frequency drive connected to the HEX fan. Finally, an extensive network of control valves is installed to easily change the operation mode of the system. More specifically, the configuration depicted in Fig. 4 offers the following options:

- to by-pass the thermal load (i.e. the air-cooled HEX or the ORC) during start-up periods so as to accelerate the heating of the HTF in the solar field;
- to remove air which could be trapped at high points of the HTF circuit;
- to drain out all the fluid in the system and to store it in the reservoir at night or during long standby periods;
- to by-pass the buffer tank in order to decrease the thermal inertia of the system;
- to dis/connect an auxiliary TES in parallel with the solar field and the thermal load;
- to dis/connect an auxiliary heat source (e.g. an electric resistance or a biomass boiler) in series with the solar field;
- to switch between the ORC or another thermal load to dissipate energy from the solar collectors.

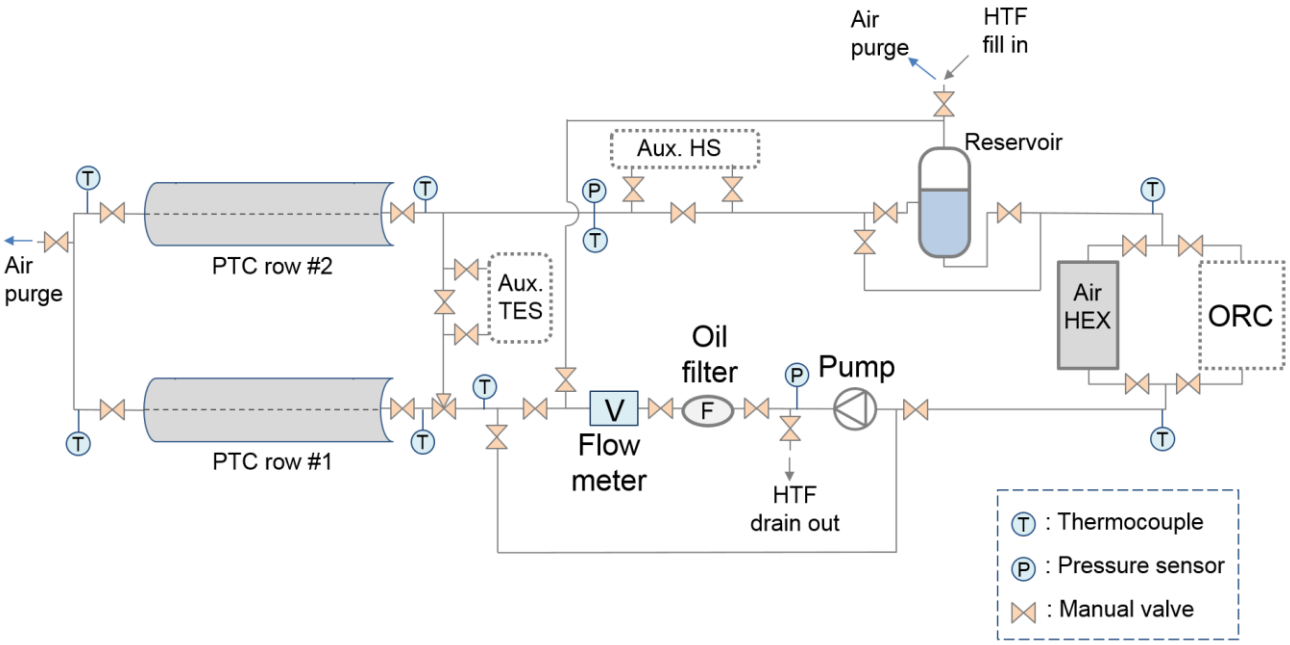


*Fig. 4. Piping and instrumentation diagram of the HTF circuit of Sun2Power.*

To ensure a minimum hydrostatic pressure through the HTF circuit, a high-point pipe riser is installed at the solar field outlet[1]. Such configuration ensures the absence of air in the receiver tubes which would cause a hazardous increase of the pipe temperatures. Finally, most of the HTF circuit components are installed above a secondary containment berm to avoid any loss of fluid in case of leakage. For additional information regarding the HTF circuit, please refer to [12]

## 2.3 Data acquisition

In addition to the collectors and the HTF circuit components, the test rig features an array of sensors and an acquisition system to record the solar field performance when in operation. As depicted in Fig. 4, T-type thermocouples are installed at key locations of the system while the thermal oil volume flow rate is measured with a standard multi-jet flow meter (MTH DN32-260 MID). Bourdon pressure gauges are also included to detect any overpressure in the HTF loop. Regarding the solar resource, solar direct normal irradiance (DNI) is measured by means of a photodiode-based Licor LI-200 pyranometer within a collimator tube mounted on a 2-axis tracking stage designed and built by STG International. Finally, a weather station installed onsite gives information about the local GHI, the ambient temperature, the wind speed/direction and the air humidity.

# 3. Experimental measurements

Preliminary tests of the solar field were performed in August 2017 and a typical day of experiments is depicted in Fig. 5. During the tests, the solar system is driven over different operating conditions by changing the HTF mass flow rate and the thermal load of the air-cooler. Out of the raw dynamic data, a set of 14 quasi steady-state points are obtained by averaging the measurements in stabilized regimes. The system is considered in quasi steady-state operation when deviations in the temperatures, HTF flow rate and solar resource remain smaller than specified thresholds during at least 4 times the residence period of the fluid in the PTC absorber tubes [16]. The operating conditions covered by the dataset as well as the thresholds used to define the steady-state points are summarized in Table1.

[1] Before entering the reservoir, the circuit features a vertical ∩-shaped pipe (2m height) which forces a column of liquid and thus ensures the entire solar field to be filled by liquid HTF.

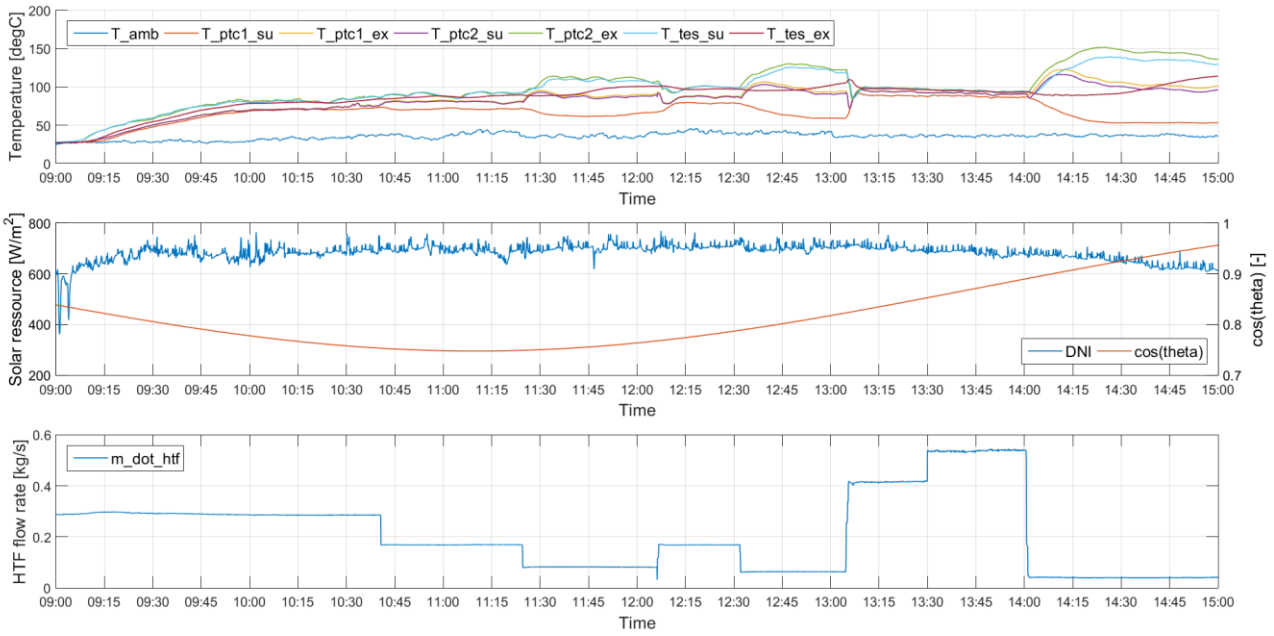


*Fig. 5. Experimental measurements gathered on the Sun2Power solar field on August 29th 2017.*

Using these quasi steady-state points, the performance of each row of parabolic trough collectors is evaluated in terms of the collection efficiency $\eta_{PTC}$, i.e.

$$\eta_{PTC} = \frac{\dot{Q}_{htf}}{\dot{Q}_{sol}} = \frac{\dot{m}_{htf}.\overline{cp}_{htf}.(T_{PTC,ex} - T_{PTC,su})}{DNI.\cos(\theta_{inc}).A_{ptc}}, \qquad (2)$$

where $\dot{Q}_{sol}$ is the useful radiant solar power captured by solar field, $\dot{Q}_{htf}$ is the effective heat transferred to the fluid, DNI is the solar direct normal irradiance, $\theta_{inc}$ is the solar rays incidence angle and $A_{ptc}$ it the effective aperture of the solar field. The collection efficiency recorded for the solar field is depicted in Fig. 6. Large measurements uncertainties are observed for points where the temperature glide in the solar field is small (< 5°C). But even considering these uncertainties, the overall performance of the solar field is low with a maximum collection efficiency of 27%. Fig. 6 also shows that there is not a strong influence of the fluid mean temperature on the PTC efficiency, which indicates that most losses result from optical issues and not from heat losses to the ambient. In order to better investigate the various sources of losses, a deterministic model of the solar field is developed and exercised in the next section.

*Table 1. Range of operating conditions covered by the experimental database.*

| Variable | [Unit] | Min. value | Max. value | Steady-state thresholds |
|---|---|---|---|---|
| $m_{dot,htf}$ | [kg/s] | 0.04 | 0.5 | ±1% rel. |
| $T_{ptc1,su}$ | [°C] | 53.2 | 87.8 | ±1 |
| $T_{ptc1,ex}$ | [°C] | 80.6 | 101.2 | ±1 |
| $T_{ptc2,su}$ | [°C] | 80.6 | 101.2 | ±1 |
| $T_{ptc2,ex}$ | [°C] | 78.1 | 144.3 | ±1 |
| DNI | [W/m²] | 590 | 710 | ±2% rel. |
| $\cos(\theta_{inc})$ | [-] | 0.74 | 0.94 | ±2% rel. |
| $T_{amb}$ | [°C] | 19 | 27 | ±1 |
| $Q_{dot,ptc}$ | [kW] | 7.31 | 8.75 | n.a. |

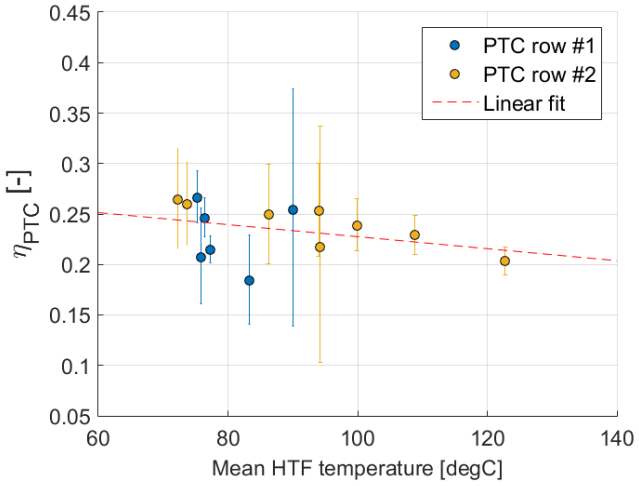


*Fig. 6. Experimental efficiency recorded for the two rows of the solar field (the brackets account for the measurements inaccuracy).*

# 4. PTC modelling and performance analysis

The parabolic trough collectors are simulated using a one-dimensional discretization of the receiver tube along its longitudinal axis. Such a simplified approach is justified by the large ratio between length and diameter of the heat collection element [17]. The temperature profile along the collectors in steady-state is evaluated by computing the HTF energy balance at each node, i.e.

$$T_{htf,i+1} = T_{htf,i} + \frac{\dot{Q}_{htf,i}}{\dot{m}_{htf} \cdot \overline{cp}_{htf,i}} \quad , \quad \forall i \in [1, N-1] \,, \tag{3}$$

where $T_{htf,i}$ represents the fluid temperature at the i[th] node in the collector. The net heat power absorbed by the fluid - $\dot{Q}_{htf,i}$ in (3) – is obtained by solving the radial energy balance of the heat collection element in each cell. To this end, the deterministic model proposed by Forristall is used[2]. As illustrated in Fig. 7a, the model accounts for each convective, conductive and radiative heat exchange between the thermal oil, the HCE components (e.g. the receiver tube and the glass envelope) and the surrounding environment. More specifically, the following system of heat balances is solved, i.e.

$$\dot{q}_{12,conv} = \dot{q}_{23,cond} \quad , \tag{4}$$

$$\dot{q}_{3SolAbs} = \dot{q}_{34,conv} + \dot{q}_{34,rad} + \dot{q}_{23,cond} \quad , \tag{5}$$

$$\dot{q}_{34,conv} + \dot{q}_{34,rad} = \dot{q}_{45,cond} \quad , \tag{6}$$

$$\dot{q}_{45,cond} + \dot{q}_{5SolAbs} = \dot{q}_{56,cond} + \dot{q}_{57,rad} \quad , \tag{7}$$

$$\dot{q}_{12,conv} = \dot{q}_{23,cond} \quad , \tag{8}$$

where the different heat transfers are depicted in Fig. 7a. Details about the model's governing equation can be found in [17] and a summary of the T13 PTC optical/geometric parameters is given in the Appendix.

[2] The model is implemented in Matlab® and an open-source version of the code is included in the ORCmKit library [18].

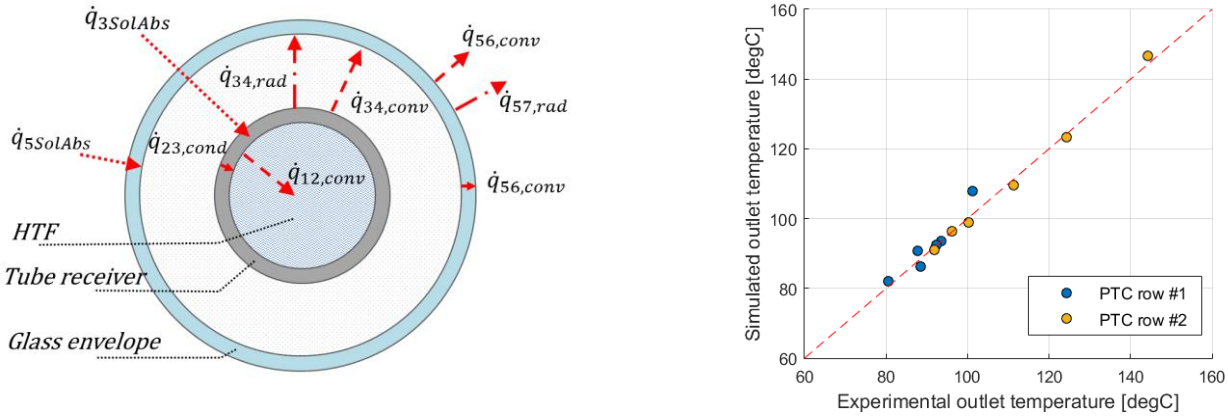


*Fig. 7. a) Radial heat balance between the HTF, the receiver tube, the glass envelope and the surrounding environment. b) Parity plot between experimental measurements and model predictions of the PTC outlet temperatures (after calibration with $K_{losses}$ = 36.9%).*

Such a deterministic model requires a perfect knowledge of the solar field properties. While most geometrical data are easily defined, thermo-optical properties of the glass envelope and the receiver tube often generate uncertainties that can affect the performance predictions. In order to resolve these uncertainties and to better replicate the experimental observations, the model may require the calibration of an empirical parameter. More specifically, the effective optical efficiency of the collectors is calculated i.e.

$$\eta_{opt} = \varepsilon_{shadow} \cdot \rho_{mirror} \cdot \varepsilon_{intercept} \cdot K_{losses} , \qquad (9)$$

where $\varepsilon_{shadow}$ characterizes shadowing losses due to the collectors structure, $\rho_{mirror}$ is the clean mirror reflectance and $\varepsilon_{intercept}$ is the design intercept factor of the T13 PTCs. These three factors are provided in the collectors technical datasheet. The last term, $K_{losses}$, is an empirical parameter which accounts for other losses not yet accounted in the model, like dirt on the mirrors, PTC end losses, or tracking inaccuracies. In order to fit the experimental measurements as depicted in Fig. 7b, an empirical value of 36.9% is found for $K_{losses}$. Once calibrated, this model is useful to better understand and predict the PTC performance in unexplored operating conditions. For instance, Fig. 8 depicts a detailed analysis of the solar energy conversion and the losses distribution for a reference point (corresponding to nominal operating conditions).

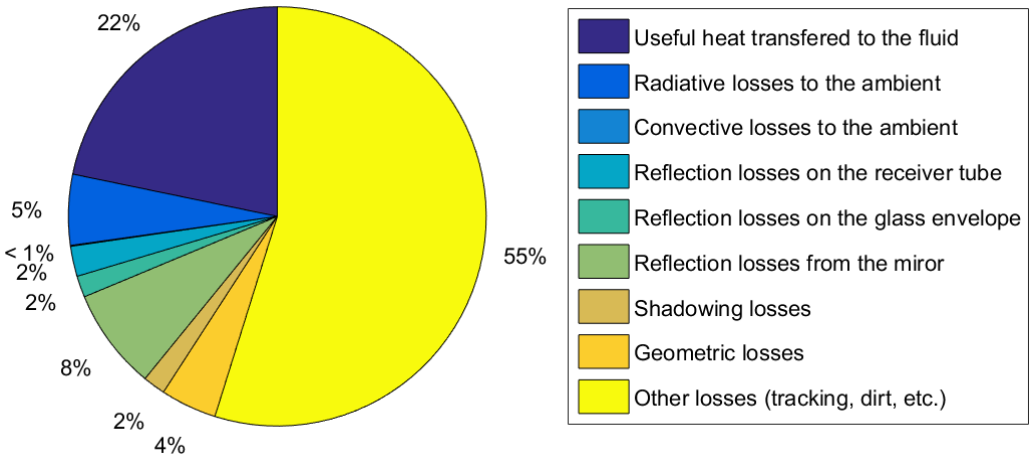


*Fig. 8. Solar energy conversion and losses distribution in the PTC for a reference point (DNI = 750W/m², $T_{htf,su}$ = 125°C, $m_{dot,htf}$ = 0.5kg/s, $T_{amb}$ = 25°C, $v_{wind}$ = 1m/s).*

For 100% of incoming energy onto the solar field, only 22% is actually transferred to the heat transfer fluid, while the remaining 78% is lost because of various phenomena. The solar collectors show a relatively good performance in terms of thermal losses. Indeed, heat losses to the environment (mostly through radiative exchanges) only represent 5% of the total incident solar energy. On the other hand, optical losses due to reflection issues or shadowing/geometric effects contribute for around 20% of the initial incoming energy. These losses can be considered as "design-related optical losses" since they result from design choices of the HCE optical properties, like the components transmittance, reflectance, absorptance or emissivities.

The remaining and the largest part of losses (around 55% of the initial solar energy) are related to the factor $K_{losses}$. Such a high contribution of "unexpected" losses cannot be explained solely because of cleanliness issues. More likely, the majority of these losses are due to a low intrinsic intercept factor in conjunction with tracking inacurracies during operation. Indeed, the tolerance angle implemented in the tracking controller ($\alpha_{tracking}$ in Eq. (1)) was relaxed during the preliminary tests for ease of operation. Instead of 0.1°, as recommended in the controller manual, a threshold of 1.5° was implemented. The prohibitive losses related to $K_{losses}$ indicate that such a large tolerance angle is likely higher than the effective acceptance angle of the collectors. This issue can be easily solved by setting a lower value of $\alpha_{tracking}$ in the tracking controller. Secondly, another source of tracking losses comes from the observed torsional deformation of the solar field along its focal axis. Since a single motor provides the torque to move an entire row of 4 collectors, frictions in the tracking mechanism tend to slightly deform the solar field between the motor location (i.e. at the centre of the row) and the rest of the row. Such torsional deformations weaken the solar concentration onto the extremities of the two rows of parabolic trough collectors. This mechanical issue can be overcome by decreasing the friction in the tracking mechanism (e.g. by improving lubrication in the moving parts, etc.).

The improvement of the tracking performance could have a major outcome on the PTC efficiency since it directly impacts the amount of solar energy concentrated onto the receiver tube. As depicted in Fig. 9, if the tracking could be improved so as to meet the design expectations (i.e. to reach a value of $K_{losses}$>0.9), the PTC efficiency could, theoretically, rise up to 55%-65% over the entire range of operating conditions. Prospective works include the implementation of such improvements and to assess experimentally the gain of PTC efficiency that can be effectively achieved.

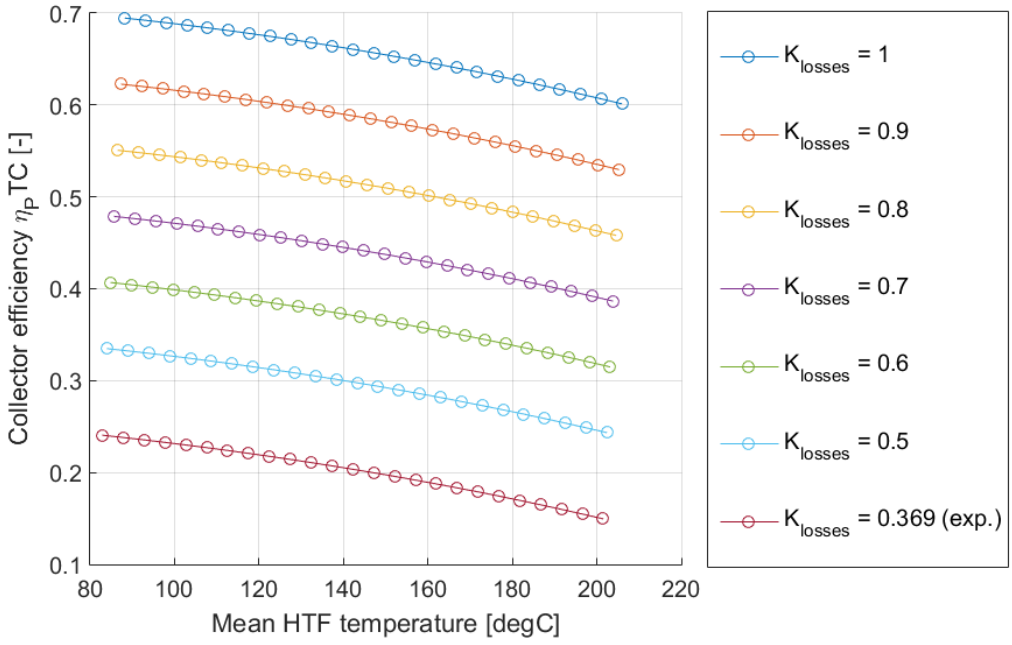


*Fig. 9. PTC efficiency in function of the fluid mean temperature for different values of $K_{losses}$.*

# 5. Conclusion

This paper presents the experimental feedback gathered on a field of parabolic trough collectors. After presenting the system and some experimental measurements, a deterministic model of the PTCs is developed to better assess their main sources of losses. The main outcomes of the paper can be summarized as follows:

- out of a first experimental campaign, a set 14 quasi steady-state points is identified to characterize the solar field performance;
- the PTC efficiency recorded experimentally is 22% on average and does not exceed 27% in the best case;
- the PTC efficiency is not much influenced by the fluid temperature which indicates that most losses result from optical issues and not from heat losses to the ambient;
- in order to fit the experimental measurements with the deterministic model proposed by Forristal, an empirical value of 36.9% is found for $K_{losses}$ (cfr. Eq. (4));
- heat losses to the ambiance occur mainly by radiation and only account for 5% of the incoming solar energy;
- "design-related" optical losses are the second source of losses and account for around 20% of the incoming solar energy;
- the majority of the losses are due to intercept/tracking errors which waste around 55% of the incoming solar energy;
- the tracking performance can be improved by decreasing (i) the tolerance angle in the tracking controller and (ii) the mechanical frictions in the tracking mechanism;
- if tracking losses could be limited to design expectations, the solar field would achieve values of efficiency up to 55%-65% over the entire range of operating conditions.

Future works include to improve the tracking accuracy and to further investigate the solar field performance. While an air-cooler is currently used as thermal load, the connection between the solar field and the ORC unit is targeted for spring 2019.

# Acknowledgement

R. Dickes thanks the Fund for Scientific Research of Belgium (F.R.S -F.N.R.S) for its financial support (research fellowship FC2349). The authors also would like to gratefully acknowledge the contributors to the Sun2Power project (CMI group, Enertime, Emerson, ACTE, Honeywell and ULiège).

# Appendix

A summary of the most relevant properties of the solar field is given in Table A.1.

*Table A.1. Summary of the solar field properties.*

| Name | Units | Value |
|---|---|---|
| General parameters | | |
| $N_{ptc}$ – Number of collectors | [-] | 8 |
| $L_{1ptc}$ – Collector length | [m] | 3.8 |
| $W_{1ptc}$ – Collector width | [m] | 2.15 |
| $A_{ptc}$ – Total collection aperture | [m²] | 65.6 |
| Solar field alignment | [-] | N-S |
| Tracking orientation | [-] | E-W |
| Receiver tube parameters | | |
| $D_{t,int}$ – internal tube diameter | [mm] | 35.1 |
| $D_{t,ext}$ – external tube diameter | [mm] | 42.4 |
| $k_t$ – tube conductivity | [W/m.K] | 17 |
| $\varepsilon_t$ – tube emissivity | [-] | 0.8 |
| $\alpha_t$ – tube absorptance | [-] | 0.92 |
| Glass envelope parameters | | |
| $D_{g,int}$ – internal envelope diameter | [mm] | 58 |
| $D_{g,ext}$ – external envelope diameter | [mm] | 66 |
| $k_g$ – envelope conductivity | [W/m.K] | 1.04 |
| $\varepsilon_g$ – envelope emissivity | [-] | 0.86 |
| $\alpha_g$ – envelope absorptance | [-] | 0.02 |
| $\tau_g$ – envelope absorptance | [-] | 0.92 |
| Other optical parameters | | |
| $\varepsilon_{shadow}$ – shadowing losses factor | [-] | 0.98 |
| $\rho_{mirror}$ – clean mirror reflectance | [-] | 0.91 |
| $\varepsilon_{intercept}$ – design intercept factor | [-] | 0.95 |
| $K_{losses}$ – unaccounted losses factor | [-] | 0.369 |

# Nomenclature

| **Letter symbols** | | **Subscripts** | |
|---|---|---|---|
| $A$ | Area, m² | amb | ambiance |
| $cp$ | Heat capacity, J/kg.K | cond | conduction |
| $D$ | Diameter, m | conv | convection |
| $K$ | Parameter, - | ex | exhaust |
| $k$ | Conductivity, W/m.K | ext | external |
| $L$ | Length, m | g | glass |
| $\dot{m}$ | Mass flow, kg/s | htf | cfr. HTF |
| $N$ | Number, - | in | inlet |
| $P$ | Pressure, Pa | inc | incident |
| $\dot{Q}$ | Heat power, W | int | internal |
| $T$ | Temperature, °C | rad | radiation |
| $v$ | Velocity, m/s | sol | solar |
| $W$ | Width, m | su | supply |
| | | t | tube |

| **Greek symbols** | | **Acronyms** | |
|---|---|---|---|
| $\alpha$ | Tolerance angle, ° | DNI | Direct Normal Irradiance |
| $\alpha$ | Absorptance, - | GHI | Global Horizontal Irradiance |
| $\varepsilon$ | Optical factor, - | HEX | Heat Exchanger |
| $\varepsilon$ | Emissivity, - | HS | Heat Source |
| $\eta$ | Efficiency, - | HTF | Heat Transfer Fluid |
| $\rho$ | Reflectivity, - | ORC | Organic Rankine Cycle |
| $\tau$ | Transmittance, - | PTC | Parabolic Trough Collector |
| $\theta$ | Angle, ° | TES | Thermal Energy Storage |

# References


[1] M. Orosz and R. Dickes, "Chapter 16. Solar thermal powered Organic Rankine Cycles," in *Organic Rankine Cycle (ORC) Power Systems: Technologies and Applications*, Woodhead Publishing Series in Energy, 2016.

[2] A. M. Delgado-Torres, "Solar thermal heat engines for water pumping: An update," *Renew. Sustain. Energy Rev.*, vol. 13, no. 2, pp. 462–472, 2009.

[3] D. Manolakos, G. Kosmadakis, S. Kyritsis, and G. Papadakis, "On site experimental evaluation of a low-temperature solar organic Rankine cycle system for RO desalination," *Sol. Energy*, vol. 83, no. 5, pp. 646–656, 2009.

[4] J. Freeman, K. Hellgardt, and C. N. Markides, "Working fluid selection and electrical performance optimisation of a domestic solar-ORC combined heat and power system for year-round operation in the UK," *Appl. Energy*, vol. 186, pp. 291–303, 2017.

[5] M. Petrollese, D. Cocco, G. Cau, M. Petrollese, and D. Cocco, "Small-scale CSP plant coupled with an ORC system for providing dispatchable power: the Ottana Solar Facility," *Energy Procedia*, vol. 129, pp. 708–715, 2017.

[6] E. Georges, S. Declaye, O. Dumont, S. Quoilin, and V. Lemort, "Design of a small-scale organic Rankine cycle engine used in a solar power plant," *Int. J. Low-Carbon Technol.*, vol. 8, pp. 34–41, 2013.

[7] R. Dickes, O. Dumont, S. Declaye, S. Quoilin, I. Bell, and V. Lemort, "Experimental investigation of an ORC system for a micro-solar power plant," in *Proceedings of the 22nd International Compressor Engineering at Purdue*, 2014.

[8] R. Dickes, O. Dumont, S. Quoilin, and V. Lemort, "Charge-sensitive modelling of organic Rankine cycle power systems for off-design performance simulation," *Appl. Energy*, vol. 212, no. January, pp. 1262–1281, 2018.

[9] "STG International." [Online]. Available: http://www.stginternational.org/.

[10] M. Orosz, P. Mathaha, A. Tsiu, B. M. Taele, L. Mabea, M. Ntee, M. Khakanyo, T. Teker, J. Stephens, and A. Mueller, "Low-cost small scale parabolic trough collector design for manufacturing and deployment in Africa," in *AIP Conference Proceedings*, 2016, vol. 1734.

[11] Alanod, "Mir4 properties." [Online]. Available: https://www.alanod.com/en/reflection/miro-sun/.

[12] J. Thiébaut, "Theoretical and experimental investigations of parabolic trough collectors for a

small-scale solar thermal power plant," University of Liège, 2017.

[13] I. Reda and A. Andreas, "Solar position algorithm for solar radiation applications," *NREL/TP-560-34302*, pp. 1–56, 2008.

[14] Pirobloc, "Datasheet of thermal oil HTF-Basic."

[15] "NG11V-PH gear pump (web page)." [Online]. Available: https://pumpbiz.com/hot-oil-gear-pump-less-motor-ng11v-ph.

[16] L. Valenzuela, R. López-Martín, and E. Zarza, "Optical and thermal performance of large-size parabolic-trough solar collectors from outdoor experiments: A test method and a case study," *Energy*, vol. 70, pp. 456–464, 2014.

[17] R. Forristall, "Heat transfer analysis and modeling of a parabolic trough solar receiver implemented in engineering equation solver," *NREL/TP-550-34169*, 2003.

[18] R. Dickes, D. Ziviani, M. de Paepe, M. van den Broek, S. Quoilin, and V. Lemort, "ORCmKit : an open-source library for organic Rankine cycle modelling and analysis," in *Proceedings of ECOS 2016*, 2016.